ACS APPLIED MATERIALS & INTERFACES

Research Article

www.acsami.org

Graphene Quantum Dots-based Photoluminescent Sensor: A Multifunctional Composite for Pesticide Detection

Erhan Zor,[†,‡,§,∥,▽] Eden Morales-Narváez,[†,▽] Alejandro Zamora-Gálvez,[†] Haluk Bingol,[∥] Mustafa Ersoz,[⊥] and Arben Merkoçi*[,†,#]

[†]ICN2—Catalan Institute of Nanoscience and Nanotechnology, Campus de la UAB, 08193 (Bellaterra) Barcelona, Spain

[‡]Science and Technology Department, A.K. Faculty of Education, Necmettin Erbakan University, Konya, 42090, Turkey

[§]Department of Chemistry, Institute of Science, Selcuk University, Konya, 42030, Turkey

[∥]Department of Chemistry, A.K. Education Faculty, Necmettin Erbakan University, Konya, 42090, Turkey

[⊥]Advanced Technology Research and Application Center, Selcuk University, Konya, 42030, Turkey

[#]ICREA—Catalan Institution for Research and Advanced Studies, Barcelona, 08010, Spain

Supporting Information

ABSTRACT: Due to their size and difficulty to obtain, cost/effective biological or synthetic receptors (e.g., antibodies or aptamers, respectively), organic toxic compounds (e.g., less than 1 kDa) are generally challenging to detect using simple platforms such as biosensors. This study reports on the synthesis and characterization of a novel multifunctional composite material, magnetic silica beads/graphene quantum dots/molecularly imprinted polypyrrole (mSGP). mSGP is engineered to specifically and effectively capture and signal small molecules due to the synergy among chemical, magnetic, and optical properties combined with molecular imprinting of tributyltin (291 Da), a hazardous compound, selected as a model analyte. Magnetic and selective properties of the mSGP composite can be exploited to capture and preconcentrate the analyte onto its surface, and its photoluminescent graphene quantum dots, which are quenched upon analyte recognition, are used to interrogate the presence of the contaminant. This multifunctional material enables a rapid, simple and sensitive platform for small molecule detection, even in complex mediums such as seawater, without any sample treatment.

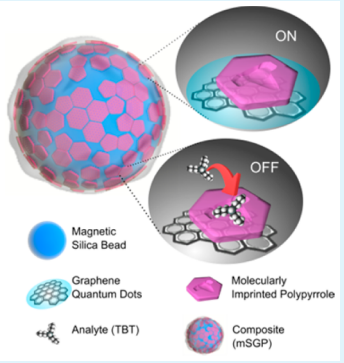

KEYWORDS: *graphene quantum dots, magnetic silica beads, molecularly imprinted polymer, multifunctional composite, small molecule detection*

1. INTRODUCTION

Small molecules such as organic toxic compounds have raised serious concerns due to not only their persistent and bioaccumulative characteristics that impact wildlife and sensitive ecosystems,[1−3] but also effects on human health, which include endocrine disruptive activity, carcinogenicity, genotoxicity, and irritancy.[4] Typically, these hazardous compounds are detected through highly sensitive and robust techniques such as high-performance liquid chromatography and mass spectrometry. However, these techniques often require expensive equipment, time-consuming sample preparation procedures, and trained personnel. As a consequence, development of simple approaches for highly specific detection of organic toxic compounds is under active research, in particular using biosensing and nanotechnology.[5]

In biosensing, biological/synthetic sensing elements (or receptors), such as antibodies or aptamers, are crucial because they selectively interact with the analyte. Owing to their size (less than 1 kDa), organic toxic compounds are not immunogenic.[6] Consequently, development of antibodies targeting these compounds is technically difficult to cope with. On the other hand, aptamers targeting organic toxic compounds have been scarcely reported and usually imply high cost and long procedures. In this context, molecularly imprinted polymers (MIPs) represent a biomimetic alternative as sensing elements.[7−10]

Moreover, nanomaterials such as graphene-related materials have received much attention in sensors and devices due to their unique electronic properties, mechanical flexibility, thermal/chemical stability, and optical properties.[11] A wide variety of optical and electrical sensing platforms based on graphene-related materials have been developed for the detection of ions, biomolecules, pathogens, and other species.[11−15] However, small molecule detection has been scarcely explored in this context. Because graphene quantum dots (GQDs) have low toxicity and are chemically inert, biocompatible, and resistant to photobleaching,[16] they are one of the emerging and promising optical nanomaterials for

Received: June 30, 2015
Accepted: August 27, 2015
Published: August 27, 2015

ACS Publications © 2015 American Chemical Society

DOI: 10.1021/acsami.5b05838
ACS Appl. Mater. Interfaces 2015, 7, 20272−20279

prospective applications in bioimaging,[17] photovoltaics,[18] chemical sensors,[19] and bio/sensors.[20] Although the electrical properties have attracted continuous and tremendous interest, the use and investigation of the photoluminescent properties of graphene-related materials remain a challenge to be completely explored.[21] Moreover, GQDs display high surface area and the carboxylic moieties at their edges provide them with water dispersibility and proper functional groups to be complexed with several compounds (including in/organic, polymeric, or biological compounds).[20] Recently, a nonmultifunctional GQDs-based composite targeting a toxic phenolic compound has been reported, however, it requires filtration procedures to assay real samples, which implies extra steps and materials during the proposed analysis.[22]

Herein, the synthesis, characterization and performance of a multifunctional composite material (mSGP) designed to detect an organic toxic compound without any sample treatment is reported. The pesticide tributyltin (TBT, 291 Da), which is genotoxic and gives rise to endocrine disruptions,[23] has been chosen as a model analyte. This composite (mSGP) consists of magnetic silica beads encapsulated by GQDs embedded in molecularly imprinted polypyrrole. Thus, the mSGP composite displays: (1) magnetic properties, which are useful for separation and preconcentration of the toxic compound; (2) water dispersibility, which is important for its processing in aqueous phase; (3) selectivity, which is pivotal in terms of selectivity and specificity; and (4) photoluminescence as an optical transducing system that is quenched by energy transfer upon analyte binding. A schematic representation of the mSGP composite and its sensing mechanism is depicted in Figure 1.

2. MATERIALS AND METHODS

2.1. Chemical and Apparatus. All commercial reagents were of analytical grade and handled according to the material safety data sheets suggested by the suppliers. Citric acid, NaOH, pyrrole, monobutyltin (MBT), dibutyltin (DBT) and tributyltin (TBT) were purchased from Sigma-Aldrich (Madrid, Spain). A solution of NH_2 functionalized magnetic silica beads (mSB S-NH_2 600) was purchased from MoBiTec (Göttingen, Germany). All aqueous solutions were freshly prepared in Milli-Q ultrapure water.

A Bruker PMA 50 (accessory coupled to Tensor 27) Fourier transformed infrared (FT-IR) spectrometer (Coventry, UK) was used to record spectra of the samples between 400 and 4000 cm^{-1}. X-ray photoelectron spectroscopy (XPS) measurements were performed using a PHOIBOS-150 analyzer/spectrometer (SPECS GmbH, Berlin, Germany). High-resolution scanning electron microscopy (SEM) images were taken on an FEI Magellan 400L SEM (Hillsboro, OR). High-resolution transmission electron microscopy (HR-TEM) images were taken with a FEI Tecnai F20 S/TEM (Hillsboro, OR). Confocal Raman measurements were performed on a Renishaw inVia Reflex (Gloucestershire, U.K.) equipped with CCD detector and a Leica microscope (Wetzlar, Germany). In order to obtain Raman images (3D-in a volume of 6 × 6 × 5 μm; x, y, z), a thin layer of the samples was deposited onto a glass slide and spectra were recorded with a 100× objective creating a 532 nm DPSS laser. Zeta potentials were measured with a Malvern Zetasizer Nano Z (Malvern, U.K.). UV−vis absorbance and fluorescence measurements were carried out using a SpectraMax M2e microplate reader (Molecular Devices, Sunnyvale, CA). AFM micrographs were obtained using a Park XE7 instrument (Suwon, Korea)

2.2. Synthesis of Multifunctional Magnetic Silica Beads/Graphene Quantum Dots/Molecular Imprinted Polypyrrole (mSGP). Synthesis of magnetic silica beads/graphene quantum dots/molecular imprinted polypyrrole (mSGP) was performed in three steps. As the first step, GQDs was prepared by directly pyrolysis of citric acid (CA).[24] Briefly, 2 g of CA was put into a 5 mL beaker and heated to 200 °C using an oil bath. After standing for 30 min at 200 °C in an oil bath, CA was liquated, the color of the liquid changed to pale yellow, and then orange, respectively. The resulting orange liquid was added drop by drop into 100 mL of 10 mg mL^{-1} NaOH solution under vigorous stirring to obtain the aqueous solution of GQDs. For the analysis processes, the GQDs solution was washed with ethanol/water (GQD solution; 80:20 v/v) and centrifuged for 10 min at 4000 rpm several times in order to remove NaOH to obtain GQDs and the precipitate was dried at 40 °C in oven for overnight. In the second step, 20 mL of GQDs solution, pyrrole (50 mM) and tributyltin (10 mM) as a template were added into the solution. Then, polypyrrole (PPy) was initiated with the addition of H_2O_2 (50 mM) under acidic conditions (pH 2) adjusted by HCl and mixed at room temperature for 24 h.[25] The color changed to pale green and then dark green indicating GQDs/PPy is obtained by in situ polymerization. The final step is the synthesis of the multifunctional mSGP composite material and removal of TBT. For this reason, after 1-ethyl-3-(3-dimenthylaminopropyl)-carbodiimide (EDC; 25 mM) and *N*-hydroxysulfosuccinimide sodium salt (Sulfo-NHS; 25 mM) were added to the GQDs/PPy solution to activate the surface carboxylic group of GQDs and mixed for 30 min at room temperature with continuous stirring,[26] 10 mL of mSB S-NH_2 (0.5 mg mL^{-1}) was added into the solution and allowed to react for 72 h at room temperature with continuous stirring. After that, TBT is removed from the polymer by washing the composite with ethanol for several times using a magnet to separate the composite after the release of TBT into supernatant. The obtained multifunctional final mSGP composite is water-soluble, photoluminescent led by GQDs, selective for TBT due to the MIP and easy to remove from the solution by its magnetic property.

2.3. Procedure for Fluorescence Measurements and Real Sample Analysis. In a typical test, a suspension of as-prepared mSGP composite (200 μL, in Milli-Q water) and different amounts of TBT (usually from 10 ppb to 10 ppm) or the other possible interferents such as MBT and DBT were added into a 96-well fluorescence microplate and incubated during 45 min to capture the analyte. The excitation wavelength was 365 nm. For the real sample analysis measurements, TBT, MBT, and DBT were added into the seawater solution with suspended mSGP. Then, mSGP was separated from the

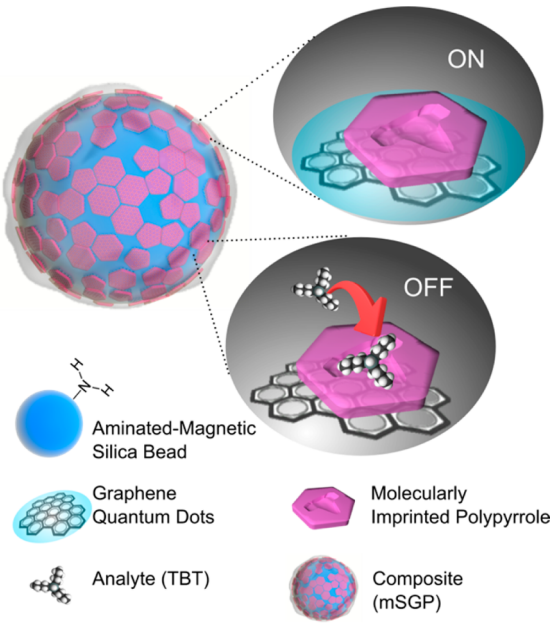

Figure 1. Schematic representation of the mSGP composite and its sensing mechanism. The concept is based on turn-off in photoluminescence of mSGP. Once pesticide (TBT) is selectively captured by the cavities of the molecularly imprinted polymer, photoluminescent GQDs lead to an optical transducing system, that is, GQDs are quenched upon analyte recognition.

DOI: 10.1021/acsami.5b05838
ACS Appl. Mater. Interfaces 2015, 7, 20272−20279

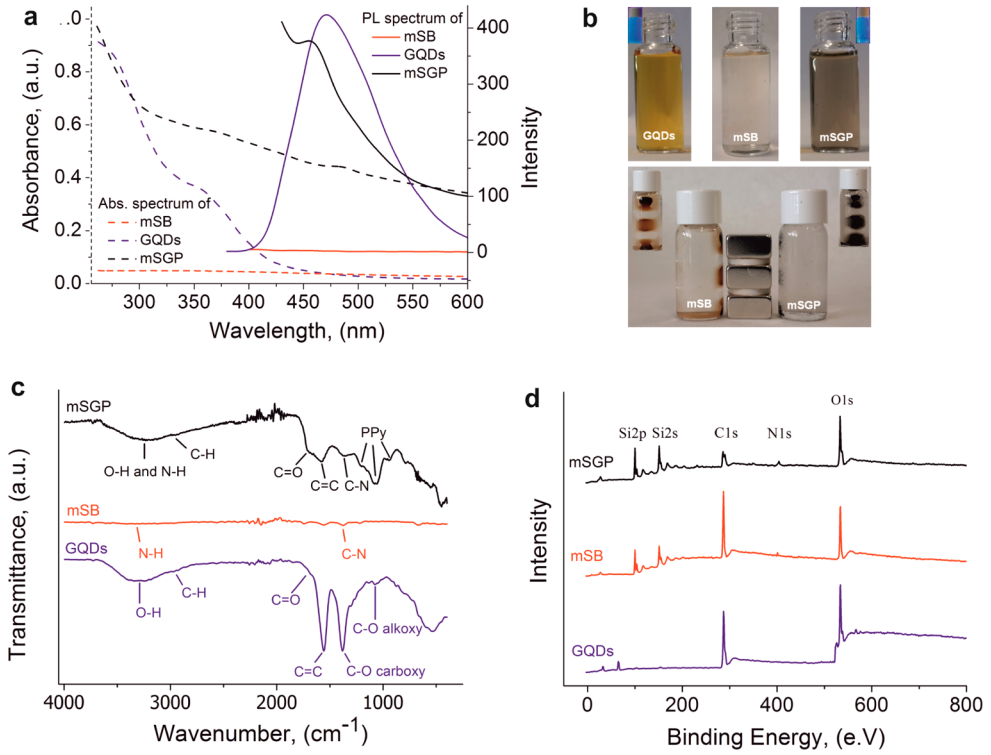

Figure 2. Spectroscopic characterization of the mSGP composite; (a) UV−vis and photoluminescent spectra, (b) the solutions and magnetic characters in water, (c) FT-IR spectra, and (d) XPS spectra of GQDs, mSB, and mSGP.

seawater solution using a magnet and resuspended in 200 μL of distilled water, and fluorescence spectra were recorded.

2.4. Quantum Yield Determination. The quantum yields (QYs) of the GQDs and mSGP were determined by using quinine sulfate (QY = 0.54 in 0.1 M H_2SO_4) as the standard sample[27] and were calculated according to the following equation;

$$Q_x = Q_{st}\frac{I_x}{I_{st}}\frac{A_{st}}{A_x}\frac{n_x^2}{n_{st}^2} \quad (1)$$

where Q refers to quantum yield, I is the measured emission intensity, A is the extinction, and n is the refractive index. The subscript "st" belongs to the standard solution, and "x" represents the sample.

3. RESULTS AND DISCUSSION

3.1. Characterization. The characterization of the composite material was performed by ultraviolet−visible spectroscopy (UV−vis), photoluminescent spectra, Fourier transform infrared spectroscopy (FT-IR), X-ray photoelectron spectroscopy (XPS), scanning electron microscopy (SEM), high resolution transmission electron microscopy (HR-TEM), and confocal Raman microscopy techniques.

3.1.1. UV−Vis Absorption, Photoluminescence Spectra, and Colloidal Stability. Figure 2a shows the UV−vis absorption and photoluminescence spectra of GQDs, magnetic silica beads (mSB) and mSGP. GQDs dispersion display a maximum absorption peak at 273 nm due to the $\pi-\pi^*$ transition of aromatic C═C bonds and a typical absorption peak at 365 nm which corresponds to the $n-\pi^*$ transition of the C═O bond.[28,29] On the other hand, mSB is optically inactive, whereas mSGP shows two weak shoulders in absorption spectrum at 367 nm and at 485 nm which are respectively $n-\pi^*$ transition of the C═O bond[29] and the characteristic absorption peak of PPy.[30]

Figure 2b shows the solutions of GQDs (yellow), mSB (pale yellow-brown), and mSGP (dark green-black), which implies the final composite material is synthesized and completely different from the precursor materials. As it can be seen, both solutions of GQDs and mSGP emit blue light (at 470 and 460 nm, respectively) under 365 nm UV beam. Although both GQDs and mSGP have their maximum luminescence quantum yields (QYs) at emission wavelengths of 470 and 460 nm, the GQDs show much stronger luminescence than the mSGP under excitation of 365 nm light. The QYs of GQDs and mSGP at 365 nm were calculated to be about 3.9% and 1.1%, respectively. The drop in the QY of the composite can be attributed to the covalent functionalization of the GQDs with magnetic silica beads containing NH_2 groups, which modifies the original moieties in the GQDs. Additionally, the vials shown in Figure 2b display the magnetic properties of mSB and mSGP (applying a permanent magnetic field with the triple magnets).

It should be noted that this magnetic property not only is crucial to remove the template molecule after MIP synthesis (or subsequently capturing the analyte) but also may be used as a preconcentration process to enrich the concentration of samples with low content of analyte. Moreover, the zeta potential measurement (Figure S1a) indicates that the silica beads are positively charged in water with a zeta potential of + 22.60 ± 0.86 mV due to the amine groups on the surface of silica beads, whereas mSGP is negatively charged with a stable zeta potential value of −47.10 ± 2.23 mV due to the GQDs which have oxygen containing groups such as −OH and −COOH, as shown in Figure S1b.

3.1.2. Fourier Transform Infrared Spectroscopy (FT-IR) and X-ray Photoelectron Spectroscopy (XPS) Analysis. FT-IR analysis of GQDs, mSB and mSGP was represented in Figure 2c. The broad bands at 3243−3291 cm^{-1} are ascribed to − OH and − NH groups stretching vibration.[24] The peak at 2956

DOI: 10.1021/acsami.5b05838
ACS Appl. Mater. Interfaces 2015, 7, 20272−20279

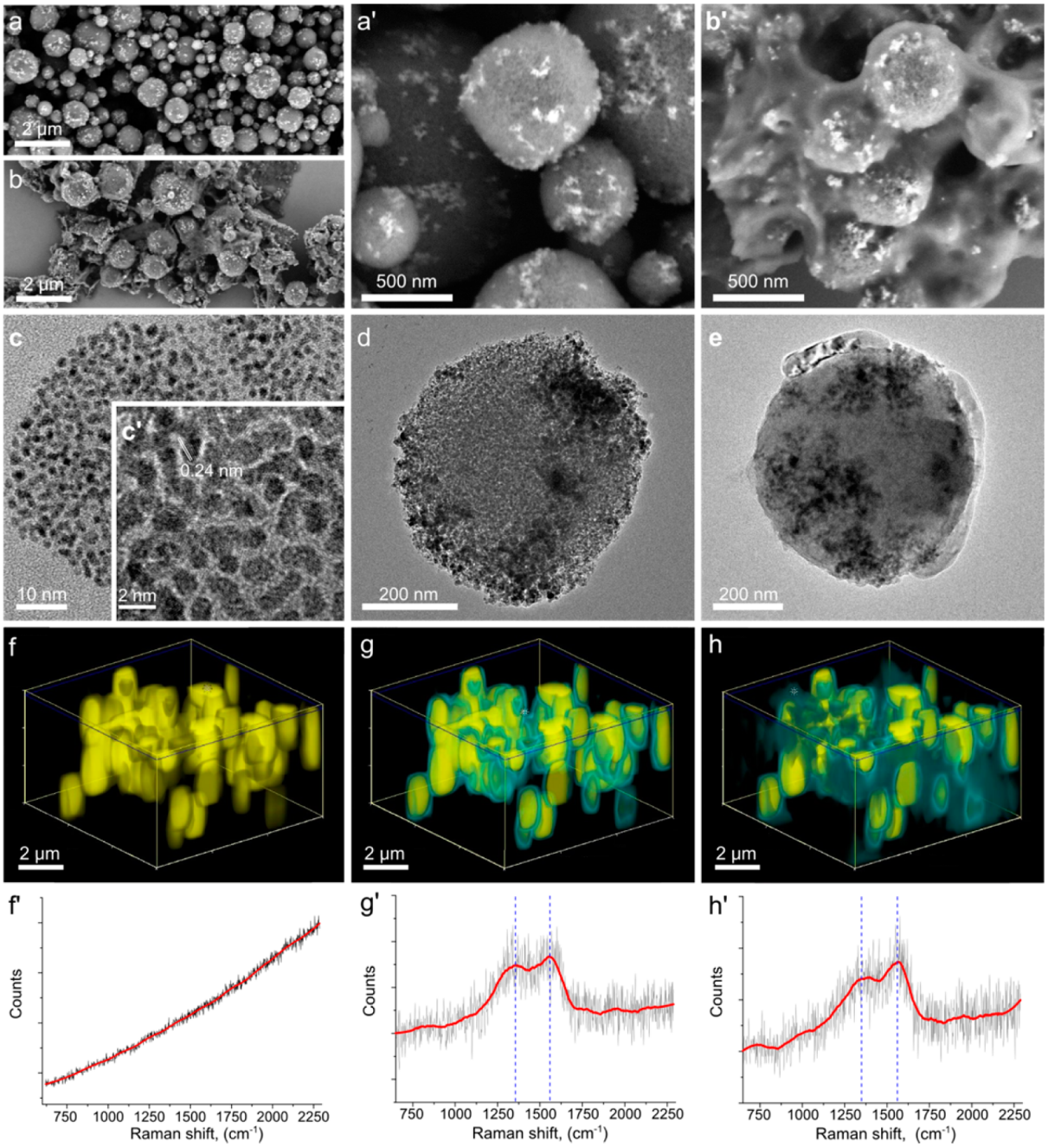

Figure 3. Images of the mSGP composite. SEM micrographs of (a and a′) mSB and (b and b′) mSGP. HRTEM micrographs of (c and c′) GQDs, (d) mSB, and (e) mSGP. 3D Raman images and Raman spectra of (f and f′) mSB, (g and g′) mSB/GQDs, and (h and h′) mSGP (Video SV1).

cm^{-1} in spectra shows the asymmetric stretching and symmetric vibrations of C−H.[24] The well-defined peak at 1565 cm^{-1} is related to bending vibrations of C═C group.[29] The peaks at 1685, 1380, and 1061 cm^{-1} were assigned to the C═O, C−O (carboxy), and C−O (alkoxy) functional groups, respectively.[29] The band at 1356 cm^{-1} belongs to C−N stretching modes. For the mSGP composite, and 1204, 1068, and 928 cm^{-1} are related to the characteristic peaks of PPy suggested the successful coating of polymer.[31] Figure S2 shows the IR spectrum of GQDs/PPy which includes the main characteristic peaks of GQDs (beside peaks of PPy) that proves the presence of carboxylic group to conjugate with magnetic silica beads.

XPS technique was used for further confirmation of the functional groups in the GQDs, mSB, and mSGP composite, and the results are given in Figure 2d. As can be seen, C 1s and O 1s signals were observed at 284 and 530 eV for GQDs.[32] XPS spectra for mSB and mSGP composite show Si 2p peaks at 99.7 and 103.9 eV (belong to $2p_{3/2}$ and $2p_{1/2}$, and SiO_2,[33] respectively) and Si 2s peaks around 151 eV.[34] N 1s peak at 400 eV was obtained beside C 1s and O 1s at 284 and 530 eV, which implies the incorporation of mSB and PPy. Also, N 1s peak intensity of composite is higher than that of mSB, which can be attributed the formation of PPy. The high-resolution C 1s spectrum of GQDs, mSB and mSGP were also performed and shown in Figure S3. GQDs show four peaks at 284, 285.0, 287.4, and 288.7 eV corresponding to C═C, C−C, C−O, and

DOI: 10.1021/acsami.5b05838
ACS Appl. Mater. Interfaces 2015, 7, 20272−20279

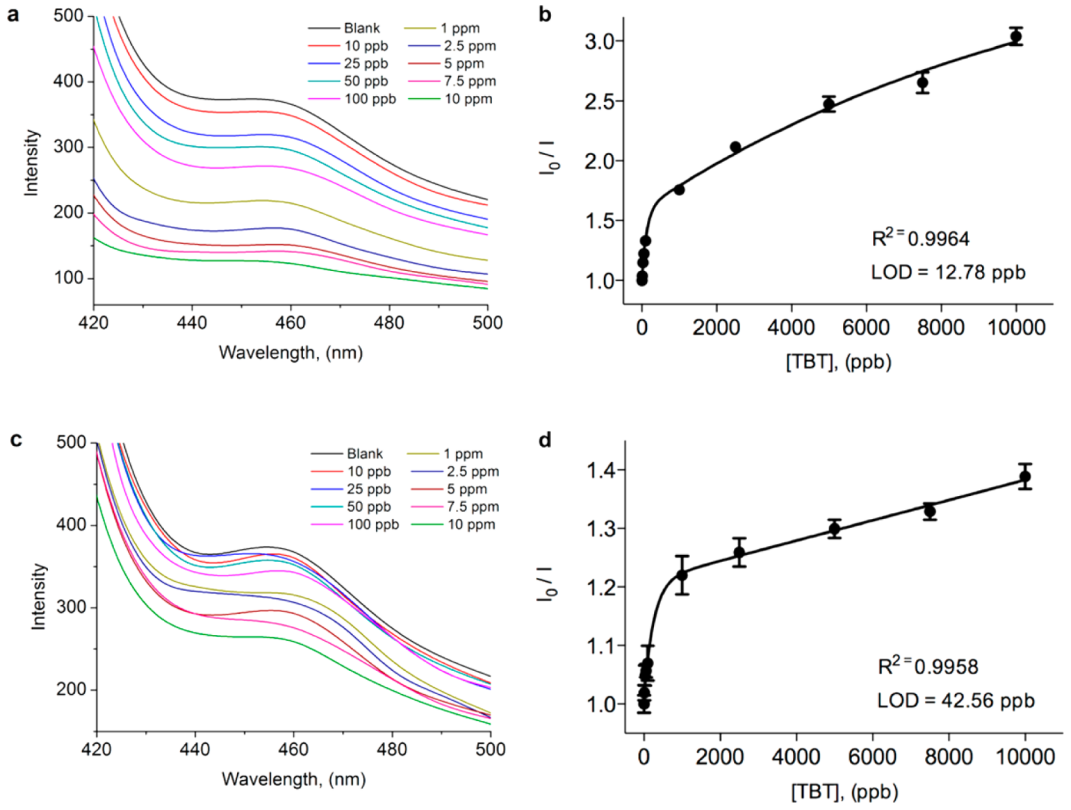

Figure 4. Behavior of the GQDs-based photoluminescent sensor. Spectral change of mSGB in the presence of TBT at different concentrations (0.0–10 ppm) in (a) pure water and (c) seawater. Nonlinear calibration curves (two phase association) for (b) pure water and (d) seawater analysis. The error bars represent the standard deviation of three parallel experiments.

COOH groups, respectively (Figure S3a). As shown in Figure S3b, mSB has two peaks at 284.5 and 285.7 eV that belong to C−C and C−N, respectively. For mSGP (Figure S3c), C 1s is deconvoluted into five unit moieties: C═C/C−C with a binding energy at 283.9 eV, C−N and C−O at 285.7 and 286.8 eV, C═O at 287.2 eV, and N−C═O at 288.5 eV, proving the chemical reaction of EDC/NHS. These results support the presence of composite and are consistent with the other spectroscopic results.

3.1.3. Scanning Electron Microscopy (SEM) and High-Resolution Transmission Electron Microscopy (HRTEM) Analysis. SEM and HRTEM were used to examine the structure of GQDs, mSB and mSGP. mSB exhibit a diameter size ranging from 200 nm to 1.2 μm (manufacturer's data, approximate values). Figure 3a,a′ and 3b,b′, respectively, show the SEM micrographs of mSB that has a porous appearance and of mSGP which exhibits a smooth appearance well-covered by polymer and GQDs. This coating can be explained by the interaction of positively charged Py molecule in its nitrogen (N) site with the negative charged GQDs due to the abundant oxygen groups such as − COOH and − OH on its edge as observed from the FTIR spectrum shown in Figure 2c.[35] Figure 3c,c′ show HRTEM micrographs of the GQDs with different magnifications. Figure S4 exhibits the size distribution of GQDs, which is uniform with an average diameter of 2.37 ± 0.39 nm. GQDs have crystallinity with lattices of 0.24 nm which are sp^2 clusters in GQDs (Figure 3c′).[26,36,37] As shown in Figure 3d, mSB has a spherical shape and a porous surface. After in situ polymerization and GQDs linkage around the mSB surfaces, the porosity disappeared due to the encapsulation of mSB by polymer matrix and GQDs (Figure 3e) indicating the formation of mSGP. Figure S5 shows the AFM image acquired in air under tapping mode and height profile of GQDs. The thicknesses of the GQDs are about 1.2 nm depicting that they assume the same structure.

3.1.4. Confocal Raman Analysis. In the following study, confocal Raman measurements were recorded in order to analyze the 3D shape of the composite material. Figure 3f,f′ display the resulting 3D Raman image of the mSBs, which are nearly ball-shaped in yellow color, and the Raman spectrum, respectively. As can be seen in Figure 3g, mSBs are surrounded by GQDs which are shown in phase with turquoise color and the corresponding Raman spectrum (the marked point with star in the figure) shows D and G bands at 1351 and 1560 cm^{-1}, which are characteristic bands for GQDs as previously reported in the literature (Figure 3g′).[38,39] The peak of D band refers to the defects and disorder in hexagonal lattice, whereas G-band is due to the vibration of sp^2 bonded carbon atoms in the 2D hexagonal lattice. The calculated I_D/I_G ratio is 0.86 which express the atomic ratio of sp^2/sp^3 carbons. The corresponding Raman image and Raman spectrum for mSGP are shown in Figure 3h,h′. The blue colored cloud-shaped material belongs to the occurring polymer with the combination of GQDs (Video SV1). The Raman spectrum shows four different peaks at around 1000, 1332, 1388, and 1566 cm^{-1}. The peaks at 1332 and 1566 cm^{-1} refer to the characteristic D and G bands of GQDs. It should be mentioned that these bands of mSGP are similar to those of GQDs which can be ascribed to the fact that the polymeric part may also have GQDs due to the in situ polymerization process. In addition, the small and broad peak around 1000 cm^{-1} can be attributed to the characteristic peak of PPy which is due to the

DOI: 10.1021/acsami.5b05838
ACS Appl. Mater. Interfaces 2015, 7, 20272−20279

bipolaron ring deformation and polaron symmetric C−H in plane bending vibration and the peak at 1388 cm^{-1} is ascribed to the ring stretching mode of PPy.[40] The calculated I_D/I_G ratio is 0.80.

3.2. Performance of the mSGP Multifunctional Composite As a Sensing Platform. *3.2.1. Sensing Principle, Optimization, and Sensitivity.* The proposed sensing platform is based on energy transfer.[41−43] Thus, the analyte, being an organometallic compound, is expected to quench the photoluminescence (PL) of the GQDs embedded within the composite in order to interrogate the absence/presence of the analyte. Aiming at researching the analytical performance of the engineered sensing platform under optimal conditions, a judicious selection of the monomer amount and the analyte incubation time was carried out. Figure 4a shows PL spectra recorded to investigate the interaction between TBT and mSGP under the optimized conditions; (1) monomer amount which concentration was chosen to be 50 mM owing to the observation of total quenching due to energy transfer and (2) incubation time that was selected as 1h because the PL intensity quenched within 45 min and after that remained almost stable (Figure S6a,b). The emission peak at 460 nm gradually decreased upon addition of increasing amounts of TBT (0.0−10 ppm) into the suspension of mSGP. The emission profile of mSGP as a function of TBT concentration was obtained as shown in Figure 4b, which exhibits a nonlinear calibration curve for increasing concentration of TBT. Limit of detection (LOD, i.e., the interpolation of the mean of the blank signal plus 3 times its standard deviation into the fitting curve) and limit of quantification (LOQ, i.e., the interpolation of the mean of the blank signal plus 10 times its standard deviation into the fitting curve) were estimated as 12.78 and 42.60 ppb.

3.2.2. Specificity. Specific and sensitive detection in practical applications of sensors is also one of the most important goals.[44] In order to confirm the ability of the sensing platform to display a selective and specific analytical performance, other organotin compounds such as monobutyltin (MBT) and dibutyltin (DBT) were chosen as interfering compounds. Figure S6c shows a series of PL spectral experiments carried out to investigate the interference of MBT and DBT. As shown in Figure S6d, no significant change (a negligible enhancement) was observed for emission intensity in the presence of MBT, while it decreased around 8.2% with the addition of 10 ppm of DBT. It is clear that mSGP had a strong response to TBT, which caused a significant change in PL intensity with a high quenching degree that is more than MBT and DBT. In addition to PL spectra, EDX of TEM proves the absence (Figure S7a) and presence of TBT as a result of attachment in the composite, as given in Figure S7b.

3.2.3. Seawater Analysis. TBT is considered one of the most toxic compounds introduced into the marine environment.[1] To prove the robustness and the potential utility of the developed sensing platform, we carried out a series of photoluminescence measurements in seawater in the presence of TBT at different concentrations, and the results are shown in Figure 4c. The emission peak at 460 nm gradually decreased with the increasing amount of TBT (0.0−10 ppm), whereas the peak was not totally quenched and the emission profile of mSGP as a function of TBT concentration is shown in Figure 4d. LODs and LOQs were calculated as 42.56 and 141.86 ppb in seawater. The coefficient of variation of the proposed seawater analysis ranges from ca. 1 to ca. 3%. On the other hand, the recovery ranges from ca. 92 to ca. 114% (Table ST1, Supporting Information). Overall, the results proved that this multifunctional composite material-based photoluminescent sensor was successfully applied in the detection of TBT even in a complex medium such as a real sample of seawater without any sample treatment.

4. CONCLUSIONS

We have developed a new simple and rapid approach for sensitive and selective optical sensing systems taking advantage of the proposed multifunctional composite material. The synthesized composite material has been characterized in detail using several imaging and spectroscopic techniques. The sensing approach is based on; (1) molecularly imprinted polypyrrole that selectively captures the analyte; (2) magnetic silica beads serving as a separation mechanism (3) water dispersibility that enables a liquid-phase-based assay and (4) graphene quantum dots which lead to an optical transducing system upon analyte recognition. In this respect, we have successfully determined the organic toxic compound TBT in water and seawater with a LOD of 12.78 and 42.56 ppb, respectively. This optical sensing concept can be extended to other small compounds as a simple platform that is capable of analyzing complex samples such as seawater without any sample treatment.

■ ASSOCIATED CONTENT

Supporting Information

The Supporting Information is available free of charge on the ACS Publications website at DOI: 10.1021/acsami.5b05838.

Zeta potential measurements, details on XPS spectra, the size distribution of GQDs, the effect of monomer amount and incubation time on PL quenching, recovery of the proposed sensing system (analysis in seawater), EDX in the absence and presence of TBT as a result of attachment in the composite (PDF)

Video SV1: 3D Raman imaging video recorded to show each material and the corresponding/individual Raman spectrum (AVI)

■ AUTHOR INFORMATION

Corresponding Author

*E-mail: arben.merkoci@icn.cat.

Author Contributions

[▽]The manuscript was written through contributions of all authors. All authors have given approval to the final version of the manuscript. These authors contributed equally.

Notes

The authors declare no competing financial interest.

■ ACKNOWLEDGMENTS

This work was supported by The European Commission Program, FP7-OCEAN, SMS Project (613844). ICN2 acknowledges support from the Severo Ochoa Program (MINECO, Grant SEV-2013-0295).

■ REFERENCES

(1) Goldberg, E. D.; Bertine, K. K. Beyond the Mussel Watch — New Directions for Monitoring Marine Pollution. *Sci. Total Environ.* **2000**, *247*, 165−174.

(2) Barbieri, R. F.; Lester, P. J.; Miller, A. S.; Ryan, K. G. A Neurotoxic Pesticide Changes the Outcome of Aggressive Interactions

DOI: 10.1021/acsami.5b05838
ACS Appl. Mater. Interfaces 2015, 7, 20272−20279

between Native and Invasive Ants. *Proc. R. Soc. London, Ser. B* **2013**, *280*, 20132157−20132157.
(3) Beketov, M. A.; Kefford, B. J.; Schäfer, R. B.; Liess, M. Pesticides Reduce Regional Biodiversity of Stream Invertebrates. *Proc. Natl. Acad. Sci. U. S. A.* **2013**, *110*, 11039−11043.
(4) Matthews, G. *Pesticides: Health, Safety and the Environment*; 1st ed.; Wiley-Blackwell: Oxford, U.K., 2006.
(5) Aragay, G.; Pino, F.; Merkoçi, A. Nanomaterials for Sensing and Destroying Pesticides. *Chem. Rev.* **2012**, *112*, 5317−5338.
(6) Brown, M. C. Antibodies: Key to a Robust Lateral Flow Immunoassay. In *Lateral Flow Immunoassay*; Wong, R.; Tse, H., Eds.; Humana Press: Totowa, NJ, 2009; pp 1−16.
(7) Whitcombe, M. J.; Chianella, I.; Larcombe, L.; Piletsky, S. A.; Noble, J.; Porter, R.; Horgan, A. The Rational Development of Molecularly Imprinted Polymer-Based Sensors for Protein Detection. *Chem. Soc. Rev.* **2011**, *40*, 1547−1571.
(8) Merkoçi, A.; Alegret, S. New Materials for Electrochemical Sensing IV. Molecular Imprinted Polymers. *TrAC, Trends Anal. Chem.* **2002**, *21*, 717−725.
(9) Lautner, G.; Kaev, J.; Reut, J.; Öpik, A.; Rappich, J.; Syritski, V.; Gyurcsányi, R. E. Selective Artificial Receptors Based on Micropatterned Surface-Imprinted Polymers for Label-Free Detection of Proteins by SPR Imaging. *Adv. Funct. Mater.* **2011**, *21*, 591−597.
(10) Shutov, R. V.; Guerreiro, A.; Moczko, E.; de Vargas-Sansalvador, I. P.; Chianella, I.; Whitcombe, M. J.; Piletsky, S. A. Introducing MINA–The Molecularly Imprinted Nanoparticle Assay. *Small* **2014**, *10*, 1086−1089.
(11) Gravagnuolo, A. M.; Morales-Narváez, E.; Longobardi, S.; da Silva, E. T.; Giardina, P.; Merkoçi, A. In Situ Production of Biofunctionalized Few-Layer Defect-Free Microsheets of Graphene. *Adv. Funct. Mater.* **2015**, *25*, 2771−2779.
(12) Morales-Narváez, E.; Merkoçi, A. Graphene Oxide as an Optical Biosensing Platform. *Adv. Mater.* **2012**, *24*, 3298−3308.
(13) Zor, E.; Bingol, H.; Ramanaviciene, A.; Ramanavicius, A.; Ersoz, M. An Electrochemical and Computational Study for Discrimination of D - and L -Cystine by Reduced. *Analyst* **2015**, *140*, 313−321.
(14) Morales-Narváez, E.; Hassan, A. R.; Merkoçi, A. Graphene Oxide as a Pathogen-Revealing Agent: Sensing with a Digital-like Response. *Angew. Chem., Int. Ed.* **2013**, *52*, 13779−13783.
(15) Liu, Y.; Dong, X.; Chen, P. Biological and Chemical Sensors Based on Graphene Materials. *Chem. Soc. Rev.* **2012**, *41*, 2283−2307.
(16) Ye, R.; Peng, Z.; Metzger, A.; Lin, J.; Mann, J. A.; Huang, K.; Xiang, C.; Fan, X.; Samuel, E. L. G.; Alemany, L. B.; Martí, A. A.; Tour, J. M. Bandgap Engineering of Coal-Derived Graphene Quantum Dots. *ACS Appl. Mater. Interfaces* **2015**, *7*, 7041−7048.
(17) Nurunnabi, M.; Khatun, Z.; Reeck, G. R.; Lee, D. Y.; Lee, Y. Photoluminescent Graphene Nanoparticles for Cancer Phototherapy and Imaging. *ACS Appl. Mater. Interfaces* **2014**, *6*, 12413−12421.
(18) Son, D. I.; Kwon, B. W.; Park, D. H.; Seo, W.-S.; Yi, Y.; Angadi, B.; Lee, C.-L.; Choi, W. K. Emissive ZnO−graphene Quantum Dots for White-Light-Emitting Diodes. *Nat. Nanotechnol.* **2012**, *7*, 465−471.
(19) Liu, J.-J.; Zhang, X.-L.; Cong, Z.-X.; Chen, Z.-T.; Yang, H.-H.; Chen, G.-N. Glutathione-Functionalized Graphene Quantum Dots as Selective Fluorescent Probes for Phosphate-Containing Metabolites. *Nanoscale* **2013**, *5*, 1810−1815.
(20) Shen, J.; Zhu, Y.; Yang, X.; Li, C. Graphene Quantum Dots: Emergent Nanolights for Bioimaging, Sensors, Catalysis and Photovoltaic Devices. *Chem. Commun.* **2012**, *48*, 3686.
(21) Li, M.; Wu, W.; Ren, W.; Cheng, H. M.; Tang, N.; Zhong, W.; Du, Y. Synthesis and Upconversion Luminescence of N-Doped Graphene Quantum Dots. *Appl. Phys. Lett.* **2012**, *101*, 103107.
(22) Zhou, Y.; Qu, Z.; Zeng, Y.; Zhou, T.; Shi, G. A Novel Composite of Graphene Quantum Dots and Molecularly Imprinted Polymer for Fluorescent Detection of Paranitrophenol. *Biosens. Bioelectron.* **2014**, *52*, 317−323.
(23) Antizar-Ladislao, B. Environmental Levels, Toxicity and Human Exposure to Tributyltin (TBT)-Contaminated Marine Environment. A Review. *Environ. Int.* **2008**, *34*, 292−308.
(24) Dong, Y.; Shao, J.; Chen, C.; Li, H.; Wang, R.; Chi, Y.; Lin, X.; Chen, G. Blue Luminescent Graphene Quantum Dots and Graphene Oxide Prepared by Tuning the Carbonization Degree of Citric Acid. *Carbon* **2012**, *50*, 4738−4743.
(25) Ramanavicius, A.; Kausaite, A.; Ramanaviciene, A.; Acaite, J.; Malinauskas, A. Redox Enzyme − Glucose Oxidase − Initiated Synthesis of Polypyrrole. *Synth. Met.* **2006**, *156*, 409−413.
(26) Zheng, X. T.; Than, A.; Ananthanaraya, A.; Kim, D. H.; Chen, P. Graphene Quantum Dots as Universal Fluorophores and Their Use in Revealing Regulated Trafficking of Insulin Receptors in Adipocytes. *ACS Nano* **2013**, *7*, 6278−6286.
(27) Tetsuka, H.; Asahi, R.; Nagoya, A.; Okamoto, K.; Tajima, I.; Ohta, R.; Okamoto, A. Optically Tunable Amino-Functionalized Graphene Quantum Dots. *Adv. Mater.* **2012**, *24*, 5333−5338.
(28) Dai, Y.; Long, H.; Wang, X.; Wang, Y.; Gu, Q.; Jiang, W.; Wang, Y.; Li, C.; Zeng, T. H.; Sun, Y.; Zeng, J. Versatile Graphene Quantum Dots with Tunable Nitrogen Doping. *Part. Part. Syst. Charact.* **2014**, *31*, 597−604.
(29) Qu, D.; Zheng, M.; Du, P.; Zhou, Y.; Zhang, L.; Li, D.; Tan, H.; Zhao, Z.; Xie, Z.; Sun, Z. Highly Luminescent S, N Co-Doped Graphene Quantum Dots with Broad Visible Absorption Bands for Visible Light Photocatalysts. *Nanoscale* **2013**, *5*, 12272−12277.
(30) Zor, E.; Saglam, M. E.; Akin, I.; Saf, A. O.; Bingol, H.; Ersoz, M. Green Synthesis of Reduced Graphene Oxide/nanopolypyrrole Composite: Characterization and H2O2 Determination in Urine. *RSC Adv.* **2014**, *4*, 12457.
(31) Zhang, J.; Zhao, X. S. Conducting Polymers Directly Coated on Reduced Graphene Oxide Sheets as High-Performance Supercapacitor Electrodes. *J. Phys. Chem. C* **2012**, *116*, 5420−5426.
(32) Qu, D.; Zheng, M.; Zhang, L.; Zhao, H.; Xie, Z.; Jing, X.; Haddad, R. E.; Fan, H.; Sun, Z. Formation Mechanism and Optimization of Highly Luminescent N-Doped Graphene Quantum Dots. *Sci. Rep.* **2014**, *4*, 5294.
(33) Radvanyi, E.; De Vito, E.; Porcher, W.; Jouanneau Si Larbi, S. An XPS/AES Comparative Study of the Surface Behaviour of Nano-Silicon Anodes for Li-Ion Batteries. *J. Anal. At. Spectrom.* **2014**, *29*, 1120.
(34) Yao, Y.; Liu, N.; McDowell, M. T.; Pasta, M.; Cui, Y. Improving the Cycling Stability of Silicon Nanowire Anodes with Conducting Polymer Coatings. *Energy Environ. Sci.* **2012**, *5*, 7927.
(35) Chen, L.; Guo, C. X.; Zhang, Q.; Lei, Y.; Xie, J.; Ee, S.; Guai, G.; Song, Q.; Li, C. M. Graphene Quantum-Dot-Doped Polypyrrole Counter Electrode for High-Performance Dye-Sensitized Solar Cells. *ACS Appl. Mater. Interfaces* **2013**, *5*, 2047−2052.
(36) Tang, L.; Ji, R.; Li, X.; Teng, K. S.; Lau, S. P. Size-Dependent Structural and Optical Characteristics of Glucose-Derived Graphene Quantum Dots. *Part. Part. Syst. Charact.* **2013**, *30*, 523−531.
(37) He, P.; Sun, J.; Tian, S.; Yang, S.; Ding, S.; Ding, G.; Xie, X.; Jiang, M. Processable Aqueous Dispersions of Graphene Stabilized by Graphene Quantum Dots. *Chem. Mater.* **2015**, *27*, 218−226.
(38) Li, Y.; Zhao, Y.; Cheng, H.; Hu, Y.; Shi, G.; Dai, L.; Qu, L. Nitrogen-Doped Graphene Quantum Dots with Oxygen-Rich Functional Groups. *J. Am. Chem. Soc.* **2012**, *134*, 15−18.
(39) Li, Y.; Hu, Y.; Zhao, Y.; Shi, G.; Deng, L.; Hou, Y.; Qu, L. An Electrochemical Avenue to Green-Luminescent Graphene Quantum Dots as Potential Electron-Acceptors for Photovoltaics. *Adv. Mater.* **2011**, *23*, 776−780.
(40) Lim, S. P.; Pandikumar, A.; Lim, Y. S.; Huang, N. M.; Lim, H. N. In-Situ Electrochemically Deposited Polypyrrole Nanoparticles Incorporated Reduced Graphene Oxide as an Efficient Counter Electrode for Platinum-Free Dye-Sensitized Solar Cells. *Sci. Rep.* **2014**, *4*, 5305.
(41) Stewart, M. H.; Huston, A. L.; Scott, A. M.; Oh, E.; Algar, W. R.; Deschamps, J. R.; Susumu, K.; Jain, V.; Prasuhn, D. E.; Blanco-Canosa, J.; Dawson, P. E.; Medintz, I. L. Competition between Förster Resonance Energy Transfer and Electron Transfer in Stoichiometrically Assembled Semiconductor Quantum Dot-Fullerene Conjugates. *ACS Nano* **2013**, *7*, 9489−9505.

DOI: 10.1021/acsami.5b05838
ACS Appl. Mater. Interfaces 2015, 7, 20272−20279

(42) Somers, R. C.; Bawendi, M. G.; Nocera, D. G. CdSe Nanocrystal Based Chem-/bio- Sensors. *Chem. Soc. Rev.* **2007**, *36*, 579−591.
(43) Algar, W. R.; Stewart, M. H.; Scott, A. M.; Moon, W. J.; Medintz, I. L. Quantum Dots as Platforms for Charge Transfer-Based Biosensing: Challenges and Opportunities. *J. Mater. Chem. B* **2014**, *2*, 7816−7827.
(44) Baaske, M. D.; Foreman, M. R.; Vollmer, F. Single-Molecule Nucleic Acid Interactions Monitored on a Label-Free Microcavity Biosensor Platform. *Nat. Nanotechnol.* **2014**, *9*, 933−939.

DOI: 10.1021/acsami.5b05838
ACS Appl. Mater. Interfaces 2015, 7, 20272−20279